Quaternary Research 73 (2010) 507–520

Contents lists available at ScienceDirect

Quaternary Research

journal homepage: www.elsevier.com/locate/yqres

Interplay between detrital and diagenetic processes since the last glacial maximum on the northwest Iberian continental shelf

Kais Jacob Mohamed [a,b,*], Daniel Rey [a], Belen Rubio [a], Federico Vilas [a], Thomas Frederichs [c]

[a] Dept. of Marine Geosciences and Land Management, University of Vigo, Faculty of Marine Sciences, Lagoas-Marcosende, 36310, Vigo, Spain
[b] Dept. Geology & Geophysics, Woods Hole Oceanographic Institution, MS #23 266 Woods Hole Rd. 02543, Woods Hole, MA, USA
[c] Dept. of Marine Geophysics, University of Bremen, P.O. Box 330 440, D-28334 Bremen, Germany

ARTICLE INFO

Article history:
Received 23 February 2009
Available online 1 April 2010

Keywords:
Environmental magnetism
Detrital input
Iberian continental shelf
Early diagenesis
Paleoclimatic evolution
Upwelling

ABSTRACT

Integrated analyses of magnetic, geochemical and textural data on six cores from the northwestern Iberian continental shelf allowed the reconstruction of the paleoenvironmental evolution of this area since the last glacial maximum (LGM). Four sedimentary units were identified, representing a succession from fluvial and subaerial settings to high and finally low-energy marine deposits subsequent to the post-LGM sea-level rise. The uppermost unit was deposited during the Holocene and its magnetic properties were controlled by the interplay between detrital input and early diagenetic reductive dissolution of magnetic minerals. Identification of a primary steady-state early diagenetic signal allowed the recognition of periods of increased detrital input, bounded by intervals of lower detrital input and intensified reductive diagenesis related to intensified upwelling in the area. These paleoenvironmental alternations are consistent with the climatic evolution of the late Holocene. During the Roman Warm Period and Medieval Warm Period, the combined effect of greater humidity and intense agricultural and mining activities led to a greater erosion and transport of detrital sediments to the shelf. In contrast, enhanced diagenetic reduction intervals, caused by upwelling intensification, were roughly coincident with the colder Dark Ages and the Little Ice Age.

Introduction

Paleoenvironmental reconstructions based on proxies from nearshore marine sedimentary environments are usually limited by their high heterogeneity, generally related to important but intermittent continental influence. Despite this important drawback at regional and global scales, the high sedimentation rates in these settings can allow for high-resolution studies. In addition, studies of nearshore sediments can also help to discriminate between local, regional and global environmental processes as well as provide robust tie points for land–ocean correlations, which are of great significance for the study of past climatic behavior.

Recent studies of northwestern Iberian continental shelf sediments have shown their potential for recording climate oscillations during the Quaternary, in particular during the Holocene (Diz et al., 2002; Desprat et al., 2003; González-Álvarez et al., 2005; Álvarez et al., 2005; Martins et al., 2006, 2007). These studies, based principally on established biological proxies (foraminifera, coccoliths, pollen, etc.), suggested that coupled solar and ocean–atmosphere forcings explain the variations in sea-surface temperature and salinity of the last 3000 yr in the Ría de Vigo (Diz et al., 2002), with a cyclicity of 1190 yr (Desprat et al., 2003). Coccolith assemblages and molecular biomarkers also allowed correlation of these climate changes to the state of the North Atlantic Oscillation (NAO) (Desprat et al., 2003; Álvarez et al., 2005), which greatly influences the climate and oceanography of the Iberian Peninsula.

Enhanced storm activity before 2850 cal yr BP was also detected by González-Álvarez et al. (2005) and associated with the change of Atlantic storm tracks in the Sub-Boreal/Sub-Atlantic transition.

Despite these studies, paleoclimate research in this area is still scarce, and the significance of the existing studies in a broader scale may be compromised by their single-site approach (González-Álvarez et al., 2005; Martins et al., 2006; Bernárdez et al., 2008), the high sedimentary heterogeneity of the continental shelf, and the influence of local continental processes. To assess the regional and global implications of the observed changes, investigations of more sites are needed in order to validate these findings as general features of the regional climate.

Environmental magnetism provides useful, rapid, cost-effective and usually non-destructive proxies to address these questions in a wide array of sedimentary environments (Thompson and Oldfield, 1986; Evans and Heller, 2003). However, the local influence of continental processes in continental shelves increases the complexity of their magnetic record compared to deeper environments and complicates their paleoclimatic interpretation.

* Corresponding author. Dept. of Marine Geosciences and Land Management, University of Vigo, Faculty of Marine Sciences, Lagoas-Marcosende, 36310, Vigo, Spain. Fax: +34 986 81 25 56.
E-mail address: kmohamed@uvigo.es (K.J. Mohamed).

0033-5894/$ – see front matter
doi:10.1016/j.yqres.2010.02.003

On the NW Iberian continental shelf this complexity can be better assessed because a) the main sources of detrital sediments are the rivers Miño and Duero, located to the south (Dias et al., 2002a); b) the catchment areas of these rivers are predominantly composed of granitic and metamorphic rocks, making the main sedimentary components siliciclastic, whilst calcareous sediments are entirely biogenic; c) reworked sediments from previous glacial cycles constitute a significant proportion of these sediments, but their variability during the Holocene is negligible given the low amplitude of sea-level oscillations in this area after 6000 cal yr BP (Durán, 2005); and d) well-studied records exist with negligible local continental influence in the outer continental margin of the adjacent Galicia Bank, in which global features have been inferred (Alonso et al., 2008; Rey et al., 2008).

Magnetic minerals typically undergo some degree of early diagenesis in nearshore settings (Liu et al., 2004; Rey et al., 2005), the extent of which depends on the balance between the export of organic matter to the sediment, sedimentation rate and oxygenation of interstitial waters. Early diagenetic dissolution of the ferrimagnetic iron oxides usually erases the original detrital magnetic signal. In some instances, its time variability holds significant paleoenvironmental information (Larrasoaña et al., 2003) which can be used as a tracer for processes like upwelling.

We present paleoenvironmental results extending back to the late Pleistocene based on magnetic, textural and geochemical properties of six cores from the NW Iberian continental shelf. A clear and spatially traceable magnetic signal related to the Roman and Medieval Warm Periods (RWP and MWP) was observed and interpreted as enhanced fluvial discharge during these intervals. These periods were bounded by zones of enhanced diagenetic alteration. This climatic signal was heavily degraded before 2500 cal yr BP by the continued progression of redoxomorphic early diagenesis with depth, rather than to climatically forced enhancement of reducing conditions.

Setting

The surficial sediments in the study area comprise an heterogeneous mixture of relict and reworked siliciclastic sands (Rey, 1993) and generally finer sediments supplied by the southern Miño and Duero rivers (Fig. 1), the latter contributing *ca.* 79% of the total fluvial input to the area (Dias et al., 2002a). The contributions of coarse material from adjacent areas like the Rías Baixas is negligible, since these former fluvial valleys, which flooded during the last transgression, act mostly as sediment traps for local catchment sediments (Rey, 1993; Vilas et al., 2005). In the middle shelf, the Galician Mud patch is the most distinctive geomorphological feature of the area. Its predominantly muddy composition stands out in the otherwise sandy shelf, while its elongated morphology parallel to the coast on the middle shelf suggests the action of along-shore sediment transport processes.

Carbonate sediments are entirely biogenic and occasionally reach local accumulations of more than 30% as a result of wave segregation (Vilas et al., 2005). This biogenic component reflects the high productivity associated with the seasonal upwelling in this region (Fraga, 1981).

The climate and oceanography of this region is influenced by the state of the NAO, which is determined by the balance between the Icelandic low and the Azores high pressure systems (Hurrell et al., 2001). The NAO seasonality causes south-southwest subtropical moist winds and storms prevail from November to March, enhancing precipitation, fluvial discharge and sedimentary inputs to the continental shelf. These conditions also favor the development of the Iberian Poleward Current, which combined with the southern waves, transport these sediments northwards (Drago et al., 1998; Dias et al., 2002a). In the summer period (April–October), the reinforcement of the Azores high (positive NAO) reverses the situation and weaker northerly winds lead to a decrease in precipitation. Northerly winds also force the upwelling of nutrient-rich eastern North Atlantic Central Waters and enhance organic productivity (Fraga, 1981), which in turn increases the export of organic carbon to the sediments.

Materials and methods

Five vibrocores (Table 1 and Fig. 1) were analyzed in this study, and a detailed description of the sampling and techniques used is provided as supplementary material. The vibrocores were sampled with U-channels to measure the bulk magnetic susceptibility (κ), isothermal (IRM) and anhysteretic (ARM) remanence at 1-cm resolution. A −0.3 T back-field was subsequently stepwise imparted to calculate the remanence coercive force (B_{cr}), the S-ratios at −0.1 T ($S_{-0.1\,T}$) and −0.3 T ($S_{-0.3\,T}$) and the Hard IRM (HIRM). The ratio ARM/IRM was calculated at 0.1 T so the same coercivity populations were magnetized in both parameters.

These U-channels were then measured at the same resolution on a CORTEX X-ray fluorescence (XRF) Core-logger to obtain semiquantitative determinations of Ca, Fe, Ti, Mn, Sr, Cu, and K, and the quality of these results was assessed with discrete XRF measurements on select intervals.

The vibrocores were also sampled at 2–5 cm resolution for grain-size analyses. Total Carbon (TC), Total Inorganic Carbon (TIC) and Total Sulfur (TS) were measured in selected intervals. Total Organic Carbon (TOC) was calculated as TC − TIC, and $CaCO_3$ was obtained applying the molar ratio 8.33 to TIC.

For a more detailed rock magnetic characterization, representative samples were further analyzed to determine the temperature dependence of susceptibility up to 700°C, hysteresis, first-order reversal curves (FORC), and coercivity spectra of the IRM. FORC processing was performed with the FORCOBELLO MATLAB® routine (Winklhofer and Zimanyi, 2006) and the coercivity spectra of IRM were analyzed with IRM-CLG 1.0 (Kruiver et al., 2001).

Additional mineralogical and compositional information of the selected intervals was obtained by observations on a field emission scanning electron microscope (SEM) in backscattering mode (BS).

The age model was built from 12 ^{14}C accelerator mass spectrometer (AMS) dates of multispecific foraminifera and one conventional ^{14}C measurement of a *Lucinoma borealis* shell (Table 1). Calibration to calendar ages was performed with Calib 5.0 (Stuiver and Reimer, 1993) and the Marine Calibration Dataset Marine04 (Hughen et al., 2004).

Results

Age model

All the individual age models showed excellent chronologic coherence, spanning from the late Pleistocene (Fig. 2a) to the recent Holocene. The last glacial maximum (LGM) was represented at least in core ZV-20 (20820 ± 345 cal yr BP at 238 cm). Mean sedimentation rate was *ca.* ~0.2 m/ka, and varied between 0.16 m/ka at the top of CGPL-00-1 and 0.4 m/ka during the early Holocene in ZV-27. Nearby cores Vigo2 VB1 (Ares et al., 2008), SMP02-3 (Bernárdez et al., 2008) and KSGX 40 (Martins et al., 2006), located closer to the axis of the Galician Mud Patch (Fig. 1), also showed similar average sedimentation rates between 0.2 and 0.3 m/ka despite potential compaction differences between the three types of coring devices employed. The wide range of sedimentation rates from ~1.39 m/ka in SMP02-3 to ~0.16 m/ka in CGPL-00-1 in the 40 × 11 km region represented by these cores clearly reveal the previously undocumented short-range variability for this type of wave-dominated sediment-starved shelves. In addition, the highest sedimentation rates in the southernmost cores (Figs. 1 and 2a) after

https://doi.org/10.1016/j.yqres.2010.02.003 Published online by Cambridge University Press

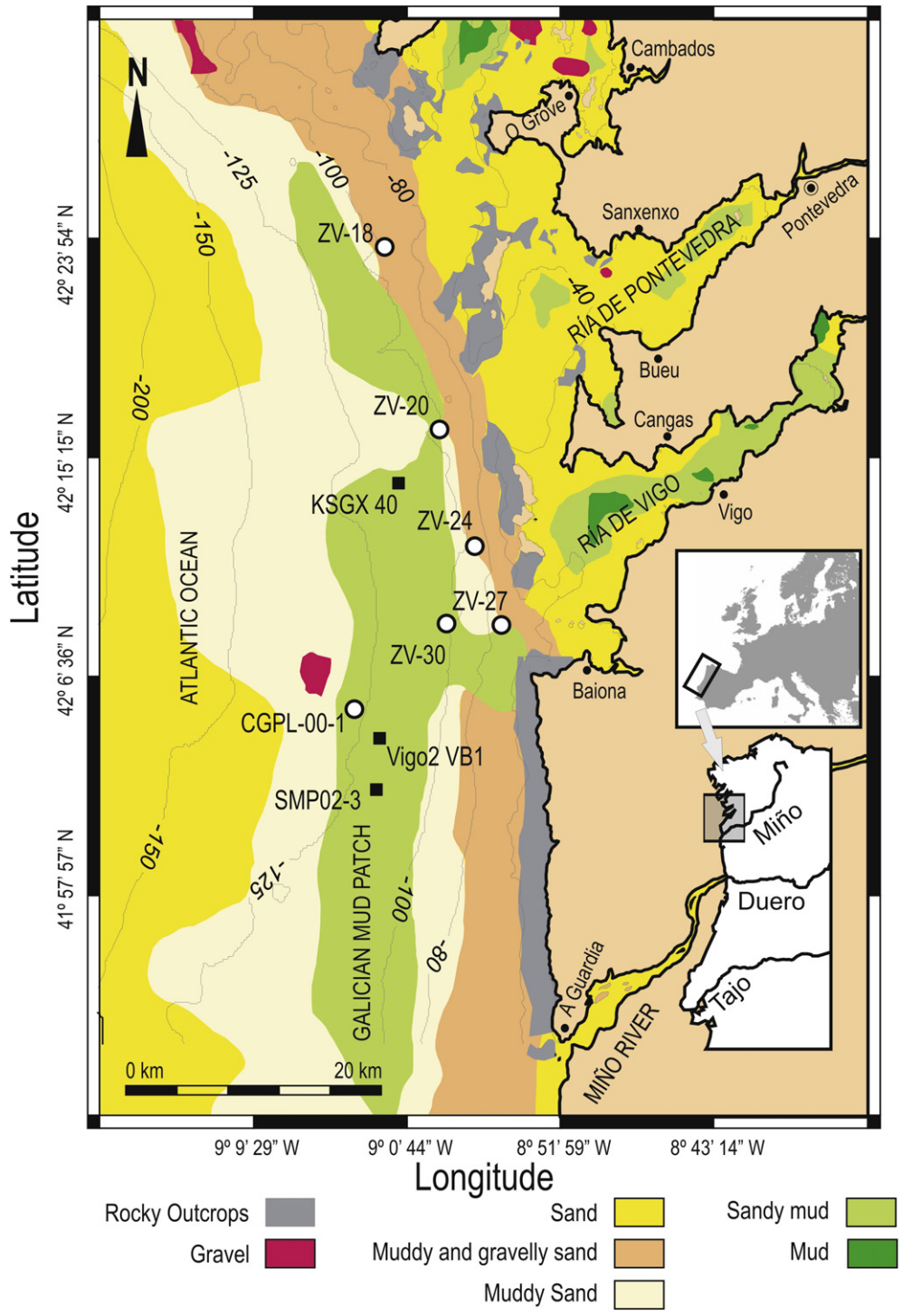

Figure 1. Location of the studied cores ZV-18, ZV-20, ZV-24, ZV-27, ZV-30, CGPL-00-1 (white circles). The positions of nearby cores Vigo2 VB1 (Ares et al., 2008), SMP02-3 (Bernárdez et al., 2008) and KSGX 40 (Martins et al., 2006) referred to in the discussion are also shown (black squares). Bathymetric contour lines in meters below sea level.

ca. 2500 cal yr BP point to the development of a depocenter to the south of the study area during the late Holocene.

Lithology

Four sedimentary Units (A to D) were identified according to the textural characteristics of the recovered sediment. Three were present in ZV-18, ZV-20 and ZV-24 and two in ZV-27 and CGPL-00-1 (Fig. 2b).

The uppermost Holocene deposit, Unit A, consisted of a fining upwards green-gray glauconitic sandy mud with biogenic carbonates. Its thickness decreased northwards, from 255 cm in ZV-30 to 50 cm in ZV-18, while its mud content increased westwards, towards the Galician Mud Patch (Figs. 1 and 2b). Deposition began during the early Holocene in the southernmost cores ZV-27 and ZV-30, whereas in ZV-20 and ZV-18 it commenced around the mid-Holocene.

Unit B was only observed in cores ZV-24, ZV-20 and ZV-18. It comprised a mixture of yellow-orange biogenic gravely sand and quartz-rich fine sand with glauconites. It ranged from 40–50 cm thick in ZV-18 to 125 cm in ZV-20. In this core, an alternation of light and dark sediments was related to three fining upwards sequences similar

https://doi.org/10.1016/j.yqres.2010.02.003 Published online by Cambridge University Press

Table 1
Chronology of the cores (2σ ranges).

Core	Coring device	Depth (cm)	Laboratory code	^{14}C AMS age (^{14}C yr BP)	Calendar age (cal yr BP)	Calendar age (cal yr BC/AD)	δ^{13}C (‰)	Reference
ZV-20		12	GX-31613-AMS	1030 ± 40	530–664	1286 AD – 1420 AD	−1.6	This work
	Vibrocore	70	GX-31614-AMS	3630 ± 50	3400–3670	1720 BC – 1450 BC	−0.7	
		238	GX-31616-AMS	18010 ± 90	20470–21160	19210 BC – 18520 BC	0.1	
ZV-27		18	GX-30666-AMS	1480 ± 30	940–1121	829 AD – 1010 AD	−2.1	This work
		64	GX-29073	3266	3266	1316 BC	−0.2	(González-Álvarez and Francés, 2005)
	Vibrocore	106	GX-30667-AMS	5160 ± 50	5410–5640	3670 BC – 3460 BC	−1.5	This work
		124	GX-30161-AMS	6450 ± 70	6750–7140	5190 BC – 4820 BC	0.8	This work
		205	GX-29684-AMS	9061	9061	7111	−2.1	(González-Álvarez and Francés, 2005)
ZV-30	Vibrocore	18	GX-31612-AMS	1580 ± 50	1020–1260	690 AD – 940 AD	−0.7	This work
		150	GX-31615-AMS	6940 ± 60	7330–7560	5610 AD – 5380 AD	−0.6	
CGPL-00-1		28	GX-28823-AMS	1260 ± 40	710–902	1048 AD – 1240 AD	*N/A*	(González-Álvarez et al., 2005)
	Gravity core	61	GX-28824-AMS	3090 ± 40	2752–2972	1023 BC – 803 BC	*N/A*	
		71	GX-28627-AMS	3100 ± 40	2759–2988	1039 BC – 810 BC	*N/A*	
VIGO2 VB1	Vibrocore	40	GX-32493-AMS	1220 ± 60	660–890	1060 AD – 1290 AD	−1.3	(Ares et al., 2008)
		140	GX-32494-AMS	2410 ± 60	1880–2220	270 BC – 70 AD	−0.9	
		230	1782	4190 ± 70	4070–4450	2500 BC – 2120 BC	−6.0	
		290	GX-32495-AMS	6110 ± 100	6310–6760	4810 BC – 4360 BC	−1.1	
SMP02-3		6	GX-30664-AMS	580 ± 30	−1[a]–400	1550 AD – 1951[a] AD	−1.7	(Bernárdez et al., 2008)
		22	GX-32033-AMS	1310 ± 40	748–935	1015 AD – 1202 AD	−1.1	
	Gravity core	150	AAR-9450	1714 ± 41	1174–1345	605 AD – 776 AD	−0.7	
		195	GX-32034-AMS	2840 ± 50	2430–2730	780 BC – 480 BC	−0.4	
		204	AAR-9451	3458 ± 50	3210–3450	1500 BC – 1260 BC	−0.6	
		255	GX-30665-AMS	4460 ± 40	4517–4787	2838 BC – 2568 BC	−0.3	
KSGX 40		40	154.383	1110 ± 40	597–753	1197 AD – 1353 AD	N/A	(Martins et al., 2006)
	Kasten core	70	154.384	2270 ± 40	1769–1988	39 BC – 181 AD	N/A	
		135	154385	3820 ± 40	3643–3883	1934 BC – 1694 BC	N/A	

^{14}C ages obtained by AMS dating of mixed foraminifera in all samples except at 71 cm of CGPL-00-1 (*G. bulloides*), 255 cm of SMP02-3 (*N. pachyderma*). The age at 64 cm in ZV-27 was obtained by conventional ^{14}C dating of a bivalve shell (*Lucinoma borealis*). N/A: δ^{13}C information not available.
[a] Calibration overlaps with the youngest reference age limit (AD 1950).

to the storm deposits found in other continental shelf settings (Lesueur et al., 2002). According to the stratigraphic position of this unit, its deposition occurred during the late Pleistocene–early Holocene.

Unit C consisted of well-sorted medium to fine siliciclastic sand with glauconites and no carbonates, and was located at the base of cores ZV-24, ZV-20 and ZV-18. Its mean grain size decreased northwards, while its thickness increased in the same direction up to the 80 cm observed in ZV-18. Based on the chronology of core ZV-20, its deposition occurred close to the LGM.

Finally, Unit D consisted of subrounded and poorly sorted siliciclastic gravely sand without carbonates. This sediment association was only found at the base of ZV-27. An age of 9060 cal yr BP immediately above the erosive contact separating Unit D from A suggests a late Pleistocene origin.

Composition

The sediments were predominantly siliciclastic, with significant biogenic $CaCO_3$ amounts in Units A and B (Figs. 3a and b). $CaCO_3$ increased downcore from 10%–20% in Unit A to up to 50% in Unit B, decreasing to ~5% in Unit C. $CaCO_3$ was strongly related to grain size and water depth, being more abundant in coarse sediments and towards the east, closer to the coast (Fig. 3b).

TOC concentrations were highest in the muddy Unit A and gradually decreased downcore (Figs. 3a and b) from ~1.8% in this unit to 0.2–0.5% at the base of Unit B, and 0.1–0.2% in Unit C. TOC also increased southwards, with maximum values in cores ZV-27 and ZV-30. TS showed a similar trend, decreasing from 0.35–0.85% in Unit A to 0.1% in Unit C. However, TS increased with depth within Unit A, mirroring the TOC trend.

Ti and Fe varied strongly between sedimentary units (Figs. 3a and b), despite their overall decreasing trend with depth. The highest concentrations were found in Unit A, where the occurrence of up to 3 peaks, especially evident in the Ti profiles, were the most prominent features. Ti also showed a strong correspondence with the mud content, coherent with the predominantly detrital origin of this fraction and the biogenic nature of the sand and gravel fractions. The lowest content was observed in Unit B as a result of its higher bioclastic content. In Unit C these elements showed a slight increase, except in ZV-20 where values similar to Unit A were attained. The ratio Fe/Ti was similar throughout Units A and C, suggesting a homogeneous composition. In Unit B the Fe/Ti increased sharply as a result of the high concentrations of bioclasts containing iron oxide coatings, as suggested by their typical orange hue.

Magnetic properties

Concentration of magnetic minerals

Bulk and carbonate-free κ, ARM and SIRM showed the same overall decreasing downcore trend (Figs. 3a and b), interrupted by several significant peaks. Unit A showed at least two maxima, A_1 and A_2, of decreasing amplitude with depth. Below A_1 a secondary peak (A_{1b}) was also observed in ZV-18, ZV-27 and CGPL-00-1. The concentration of magnetic minerals was very low in the remaining units, except in the boundary between Units A and B and in core ZV-20, and in all cases with lower amplitudes than A_1.

Magnetic mineralogy

B_{cr} and S-ratios covaried with changes in magnetic mineral concentration (Figs. 3a and b). Magnetite and titanomagnetite controlled the signal above A_1, as shown by B_{cr} around 30 mT and $S_{-0.3\,T}$ higher than 0.98. Between A_1 and A_2 the magnetomineralogical assemblage remained similar in cores ZV-18 and ZV-20. In contrast, the southernmost cores showed a magnetic hardening, suggesting higher proportions of minerals like greigite, hematite and/or goethite.

Below A_2 and down to the base of Unit A, the increase of B_{cr} to 35–57 mT in cores ZV-18 and ZV-20 and 80–100 mT in cores ZV-24 and ZV-27, as well as $S_{-0.3\,T}$ of 0.85–0.91 indicates a magnetic mineralogy very influenced by hematite and/or goethite, especially in the southernmost cores.

https://doi.org/10.1016/j.yqres.2010.02.003 Published online by Cambridge University Press

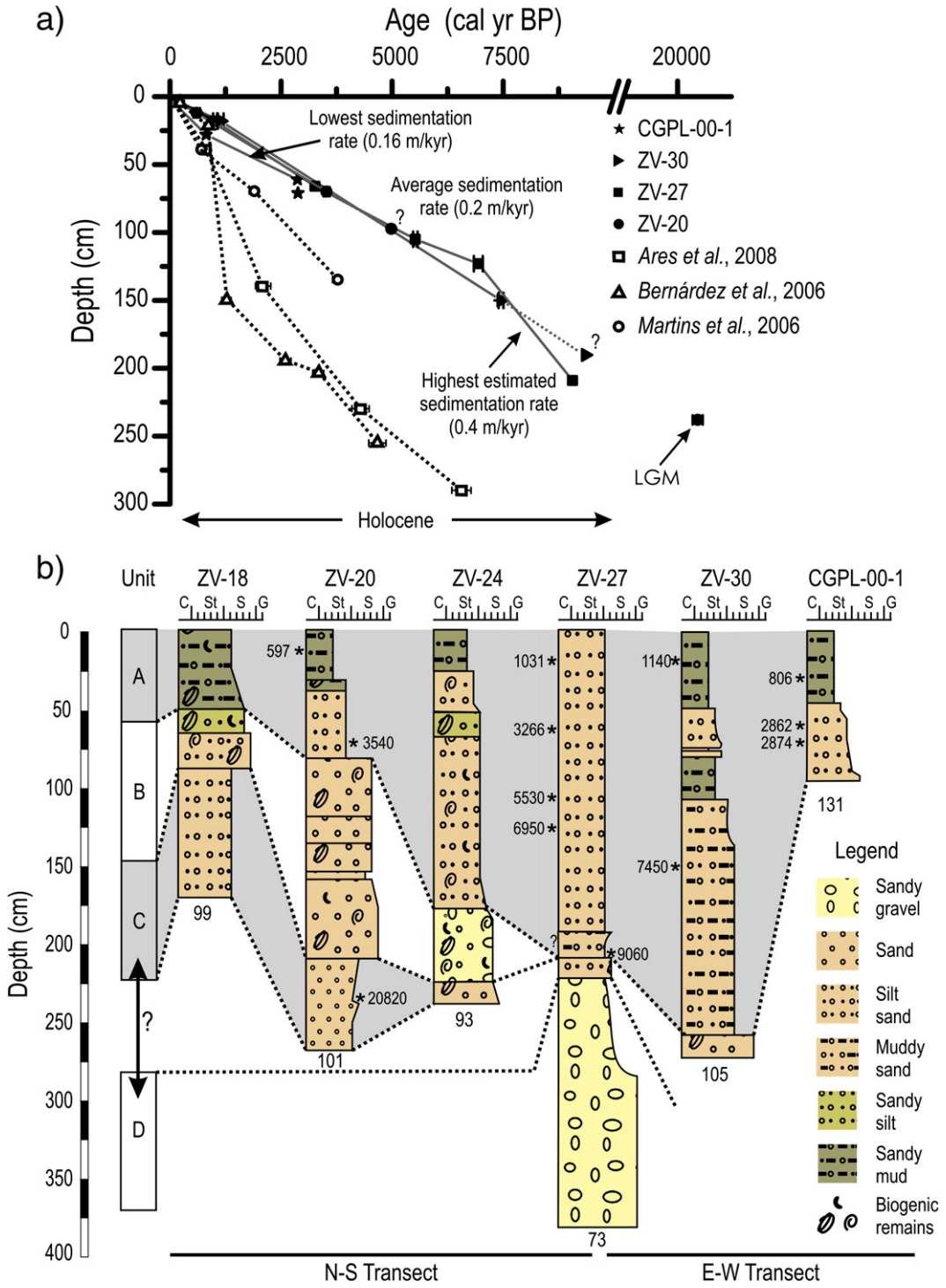

Figure 2. a) Age models for the four dated cores compared with age models for nearby cores Vigo2 VB1 (Ares et al., 2008), SMP02-3 (Bernárdez et al., 2008) and KSGX40 (Martins et al., 2006). b) Lithological correlation of the six studied cores based on the four sedimentary units established. Dated levels are marked with an asterisk and its average calendar age. Labels under the core names are C (Clay), St (Silt), S (Sand), G (Gravel). The numbers at the bottom of each log indicate the water depth at each core location.

Units B, C and most of Unit D showed compositions similar to the magnetite-dominated sediments above A_2. In Unit D, B_{cr} peaks over 100 mT and $S_{-0.3\,T}$ from 0.6 to 0.7 suggested local accumulations of hematite and/or goethite of secondary importance.

The HIRM, sensitive to hematite and goethite, was comparable to κ, SIRM and ARM (Figs. 3a and b), implying a similar origin for the observed magnetomineralogical variability. However, similar HIRM amplitudes in A_1 and A_2 suggested that hematite and/or goethite were less sensitive to the processes responsible for the downcore decrease in amplitude in κ, SIRM and ARM, which also explains the coercivity increase below A_2.

Thermomagnetic measurements showed a marked reduction in magnetization above 520°C (Fig. 4a) that rapidly decreased to *ca.* 0 at 580°C, the Curie temperature of pure magnetite. This confirms the predominance of this mineral in Unit A sediments with high concentration-dependent magnetic signals. In sediments below A_2, magnetization increased from 400 to 500°C and dropped quickly to 0 at 580°C. This behavior is typical of high-temperature oxidation

https://doi.org/10.1016/j.yqres.2010.02.003 Published online by Cambridge University Press

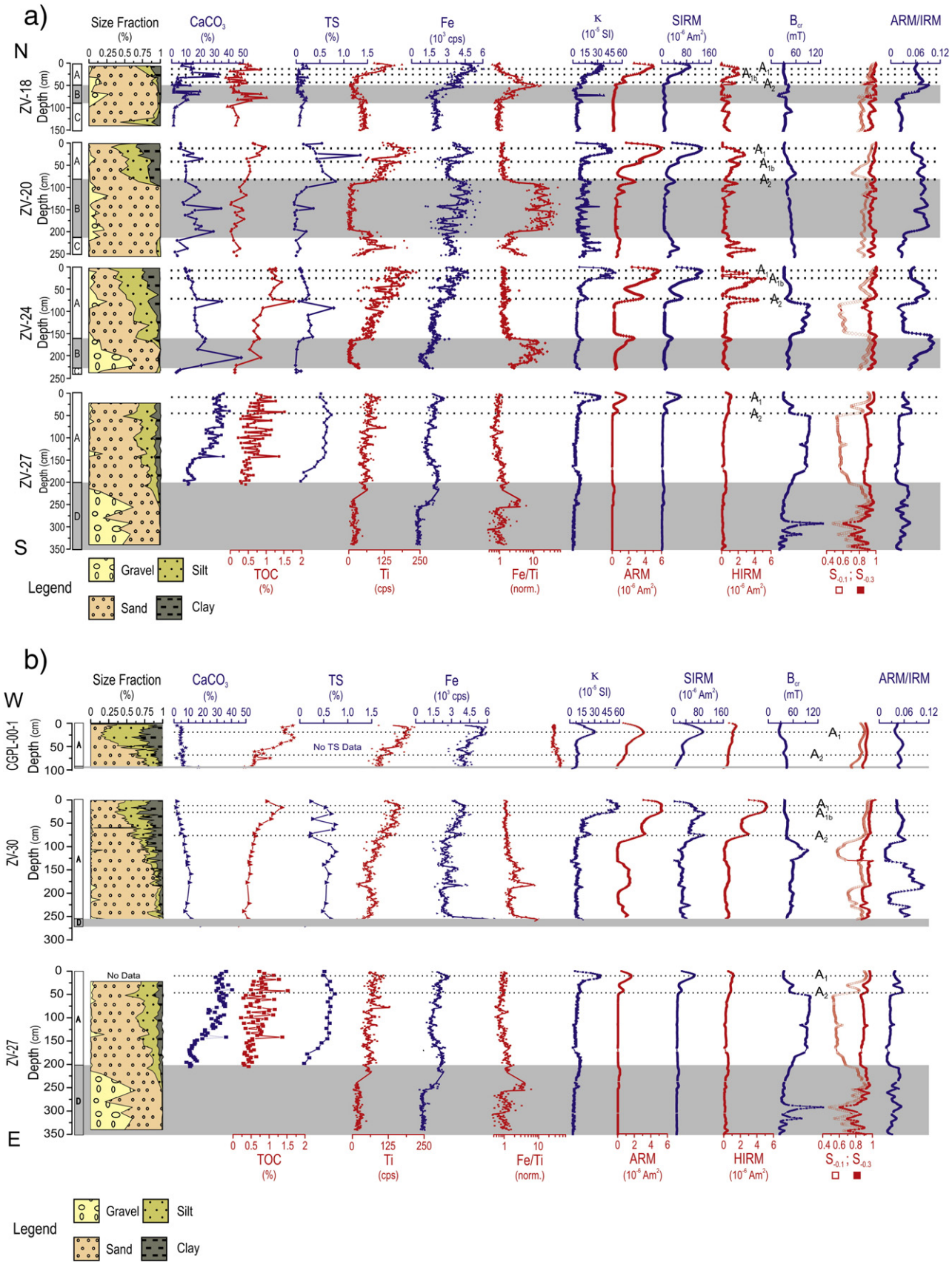

Figure 3. Representative textural, geochemical and magnetic data of the studied cores. a) North–south transect. b) East–west transect. The column to the right of the depth scale represents the four units identified in this study. The dotted horizontal lines mark the position of the peaks A_1, A_{1b} and A_2 identified in the concentration-dependent magnetic properties of Unit A. Solid curve in Fe, Ti and Fe/Ti plots corresponds to a 4-cm moving average.

https://doi.org/10.1016/j.yqres.2010.02.003 Published online by Cambridge University Press

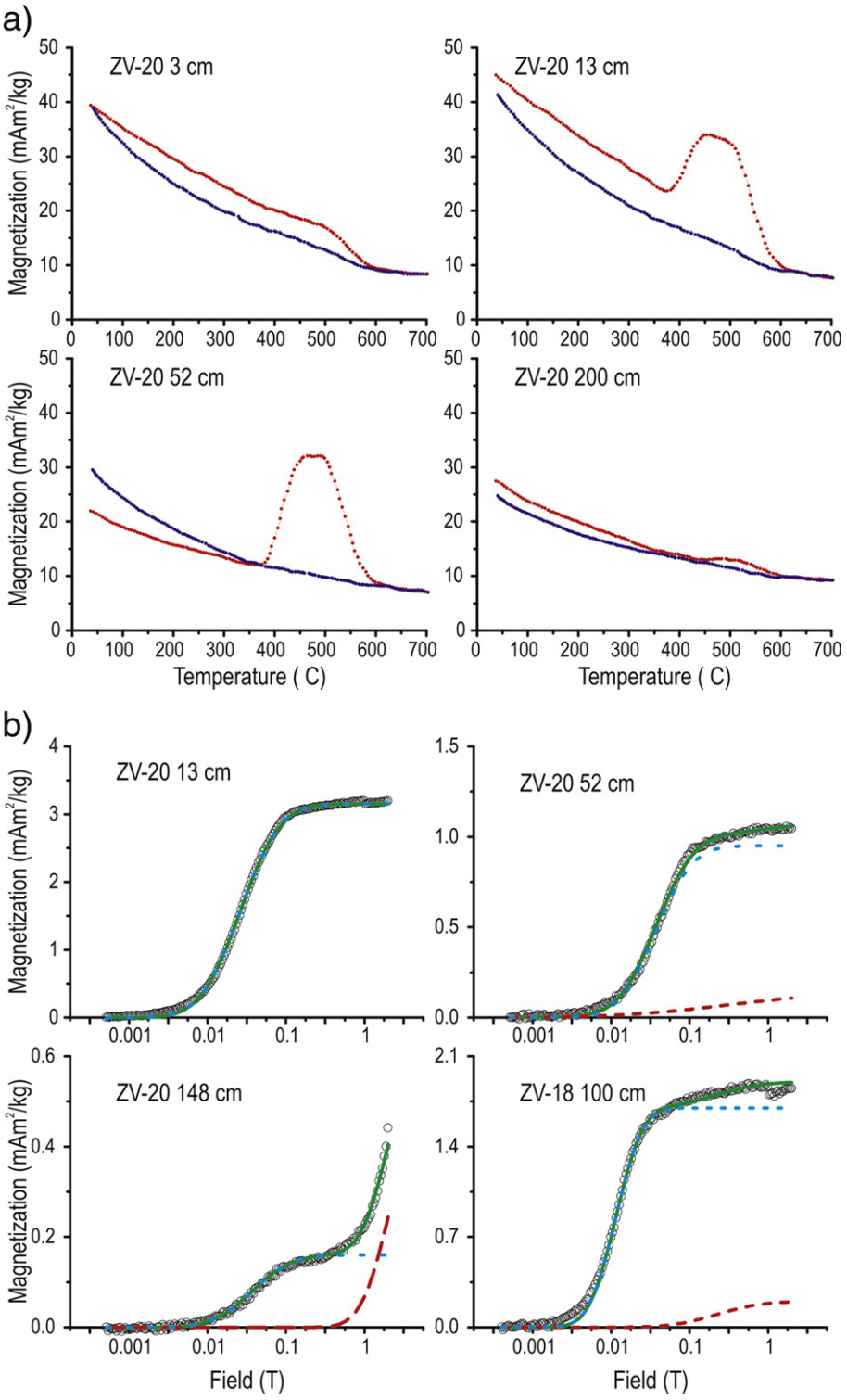

Figure 4. a) Thermomagnetic experiments (heating in red, cooling in blue). The magnetization drop near 580°C is caused by magnetite in high-concentration zones of Unit A and in Units B, C and D. The increase above 400°C is caused by the high-temperature oxidation of framboidal pyrites. b) Coercivity spectra of the IRM. The dots represent the measured data. The fit is shown as a solid green line. The blue and red dashed lines represent the dominant low-coercivity and secondary high-coercivity component, respectively. Note the logarithmic magnetic field scale. Labels in figures indicate actual core and depth interval measured.

of pyrite to magnetite (Roberts and Pillans, 1993). A double bump was frequently observed in low magnetic concentration sediments, and was interpreted as the early oxidation of framboidal pyrite followed by the oxidation of euhedral pyrite caused by the contrasting specific surfaces of the two forms of pyrite (Passier et al., 2001). SEM observations of framboidal pyrite in these sediments support this interpretation.

The IRM coercivity spectra showed the coexistence of at least two magnetic phases (Fig. 4b). In the high-concentration peaks of Unit A and in Unit C, 90–100% of the signal was carried by magnetite and

https://doi.org/10.1016/j.yqres.2010.02.003 Published online by Cambridge University Press

titanomagnetites. A secondary high-coercivity phase with mean coercivity >1 T contributed to 15–20% of the signal in the remainder of Unit A. This component contributed over 20% of the signal in Unit B, but reached its maximum contribution in Unit D and is probably carried by hematite derived from the weathering of continental igneous and metamorphic rocks. FORC measurements up to 1 T confirmed this findings, showing distributions extending up to 200 mT caused by the high-coercivity contribution of the high-coercivity phases (Fig. 5f).

Magnetic grain size

ARM/IRM also covaried with changes in magnetic concentration and mineralogy (Figs. 3a and b). The increase below A_1, more evident in ZV-24, suggested a finer magnetic grain size, although it can also be related to the precipitation of greigite under mild reducing conditions (Kao et al., 2004). Below A_2, the southernmost cores exhibited a sharp drop in ARM/IRM, and consequently a marked coarsening at these depths. This coarsening trend continued down through Unit B and C, as expected for these sandy and gravely units. Only the southernmost cores exhibited a relative fining of the magnetic mineral assemblage associated to the transition from Unit A and B. In Unit D, grain size decreases occurred in phase with the high-coercivity peaks in the lower part of this unit.

This coupling between changes in magnetic concentration, coercivity and magnetic grain size are characteristic features of sediments undergoing early diagenetic reductive dissolution (Bloemendal et al., 1993). The coarsening observed below A_2 is caused by the preferential dissolution of the smaller-sized iron oxides given their higher specific surfaces. Magnetic hardening also results from the higher resistance to reductive dissolution of hematite and goethite compared to magnetite (Bloemendal et al., 1993; Liu et al., 2004), which also explains the similar amplitudes of HIRM peaks A_1 and A_2 (Figs. 3a and b).

The Day plot (Day et al., 1977) of hysteresis data (Fig. 5a) suggested a pseudo-single domain (PSD) dominant magnetic size (1–15 μm). The high B_{cr}/B_c ratios of the low magnetic concentration sediments are caused by the increased contribution of a high-coercivity phase to the magnetomineralogical assemblage, probably hematite (Nagata and Carleton, 1987; Dunlop, 2002b). FORC diagrams of highly magnetized sediments above A_2 (Figs. 5b–c) were also consistent with a dominant PSD size (Fig. 5a), although sediments between A_1 and A_2, (Fig. 5c) exhibited a more single-domain-like (SD) behavior. Below A_2 and in Units B, C and D, multidomain (MD) grains were dominant (Figs. 5d–e). Sediments characterized by high B_{cr} showed a FORC distribution extending up to 200 mT (Fig. 5f) as a result of the increased hematite contribution.

SEM

Electron microscopy revealed that iron oxides and oxyhydroxides coexisted with iron sulfides of framboidal morphology (Fig. 6). Detrital oxides showed in many instances clear signs of dissolution, such as edging (Fig. 6a) and *in situ* fragmentation (Fig. 6b), which can explain the decreasing grain-size trend observed in the upper part of the cores. The strong diagenetic alteration of these sediments is also demonstrated by the significant replacements in carbonates (Fig. 6c) and the frequent occurrence of Fe sulfides (Fig. 6d) generally confined to organic-rich microenvironments (organic cavities, faecal pellets, etc). Energy-dispersive X-ray spectroscopy measurements confirmed pyrite as the dominant iron sulfide mineral (Fe/S around 0.66). Greigite framboids (Fig. 6d) were identified based on their Fe/S close to 0.75 and the characteristic lower brightness compared to pyrite (Roberts and Weaver, 2005; Sagnotti et al., 2005).

Discussion

Sedimentary environments since the LGM

Units A to D represent a succession of sedimentary environments controlled by the post-LGM sea-level rise. During the Flandrian transgression, fluvial (Unit D) and coastal (Unit C) subaerial environments were overlain by marine bioclastic sediments characteristic of a high-energy sedimentary regime (Unit B). After the stabilization of sea level, low-energy conditions favored deposition of muddy Unit A.

The fluvial origin of Unit D is based on its textural characteristics and its exclusive occurrence at the base of core ZV-27, which was close to the LGM incised paleochannel of the Ría de Vigo identified by García-García et al. (2005).

Unit C was deposited around the LGM, with sea level *ca.* 120 m below its current level. The lamination and high degree of sorting of this sandy unit and the absence of biogenic carbonates are typical of high-energy subaerial coastal environments (beaches, sand bars). The muddy patch dated in this unit at 238 cm is interpreted as a temporary lagoon that was subsequently filled during the progradation of sand barriers and shelf sands, as described in Vilas et al. (2010). This deposit is interpreted as reworked marine sediments from previous eustatic cycles based on the occurrence of significant amounts of glauconite, similar to the highly evolved glauconites described by Fernández-Bastero et al. (2000) at the approximate location of the studied cores. The presence of Unit C in most cores indicates a significant lateral continuity, while the fining northwards trend also indicates a southern provenance. This is consistent with results from coupled atmosphere–ocean–cryosphere models that show a NAO with predominant southerly winds in this area during the LGM (Justino and Peltier, 2005).

The textural characteristics of Unit B are similar to the palimpsests described by Rey (1993) in this area. These gravelly biogenic sands are typical of high-energy marine environments, which is coherent with its late Pleistocene–early Holocene origin, when the shallow water depth of the transgressive stage favored the reworking of sediments by waves. Furthermore, the storm-related fining upwards sequences found in core ZV-20, where this unit is best developed, suggest that most reworking occurred during peak winter storms, as can be observed at present (Dias et al., 2002b).

Finally, Unit A was deposited in a low-energy marine setting similar to the present day, starting around 5000 cal yr BP, roughly coeval with the reported sea-level stabilization for this area at ~6000 cal yr BP (Durán, 2005). Its deposition started in the early Holocene in the southernmost cores ZV-27 and ZV-30 (*ca.* 9000 and 7000 cal yr BP, respectively). This can be explained by their greater proximity to the Duero river, the main source of sediments in the area, but especially by the development of estuarine conditions at some point during the early Holocene, as suggested by the succession of fluvial (Unit D) to marine (Unit A) sediments in this area. This would enhance the efficiency of sediment trapping (Postma, 1967) and subsequently promote the earlier registration of marine sediments in this area.

Origin of the magnetic signal

Most of the magnetic variability observed in the studied region is controlled by changes in the detrital input, as evidenced by the strong correlation between the magnetic mineral concentration (κ) and the smoothed profile of Ti (Fig. 7), a common detrital proxy. The correlation coefficients (r), between κ and Ti varied between 0.60 and 0.72 considering the total core lengths, and 0.50 to 0.94 if only Unit A was considered ($p<0.0001$ in all cases). This relationship was stronger in the north ($r=0.94$ in ZV-18) than in the south ($r=0.50$ in ZV-27). Since it is well established that the main sediment sources are the

https://doi.org/10.1016/j.yqres.2010.02.003 Published online by Cambridge University Press

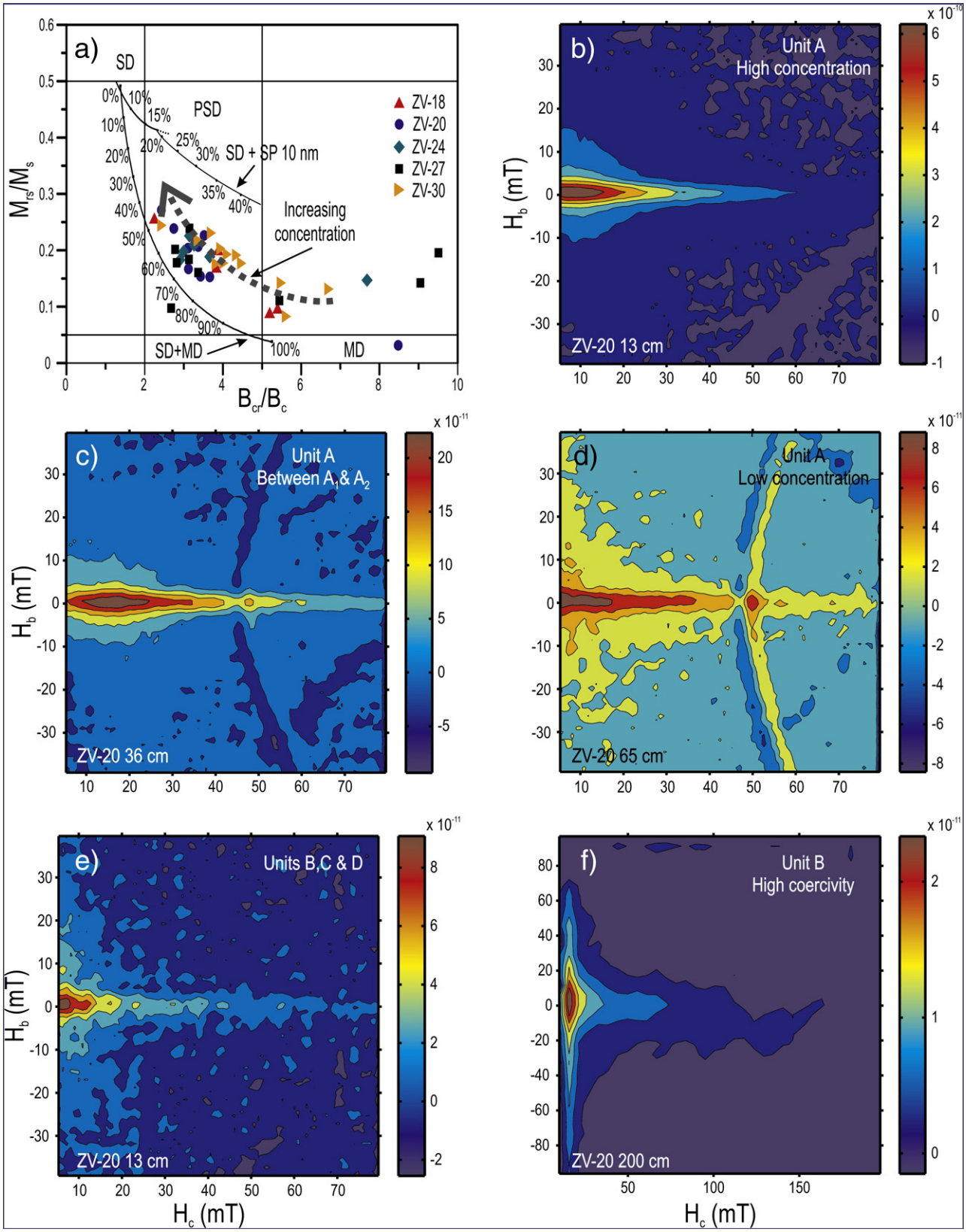

Figure 5. a) Day plot of hysteresis data showing a dominant PSD magnetic domain size. Sediments from high-concentration zones showed a trend toward smaller grain sizes with increasing concentration, which is consistent with the typical behavior observed in reductive sediments. The solid lines represent the mixing trends of the different domain states for pure magnetite (Dunlop, 2002a). b) FORC diagrams typical of high-concentration zones showing PSD-like behavior, with closed inner contours and diverging outer contours towards the origin. c) Sediments of intermediate concentration between A_1 and A_2 also exhibited PSD-like behavior. d) Low-concentration zones of Unit A showed MD behavior. The curved vertical feature appearing in c and d at 50 mT is a processing artifact. Sediments from low-concentration zones of Units B, C and D also exhibited MD behavior. Symmetry along the $H_b = 0$ axis discards any significant magnetic interaction. f) FORC distribution reaching B_c of 200 mT confirms the contribution of a high-coercivity phase in sediments from low-concentration zones. Labels inside the diagram indicate actual core and sample depth. All FORCS were produced with a smoothing factor (SF) of 4.

https://doi.org/10.1016/j.yqres.2010.02.003 Published online by Cambridge University Press

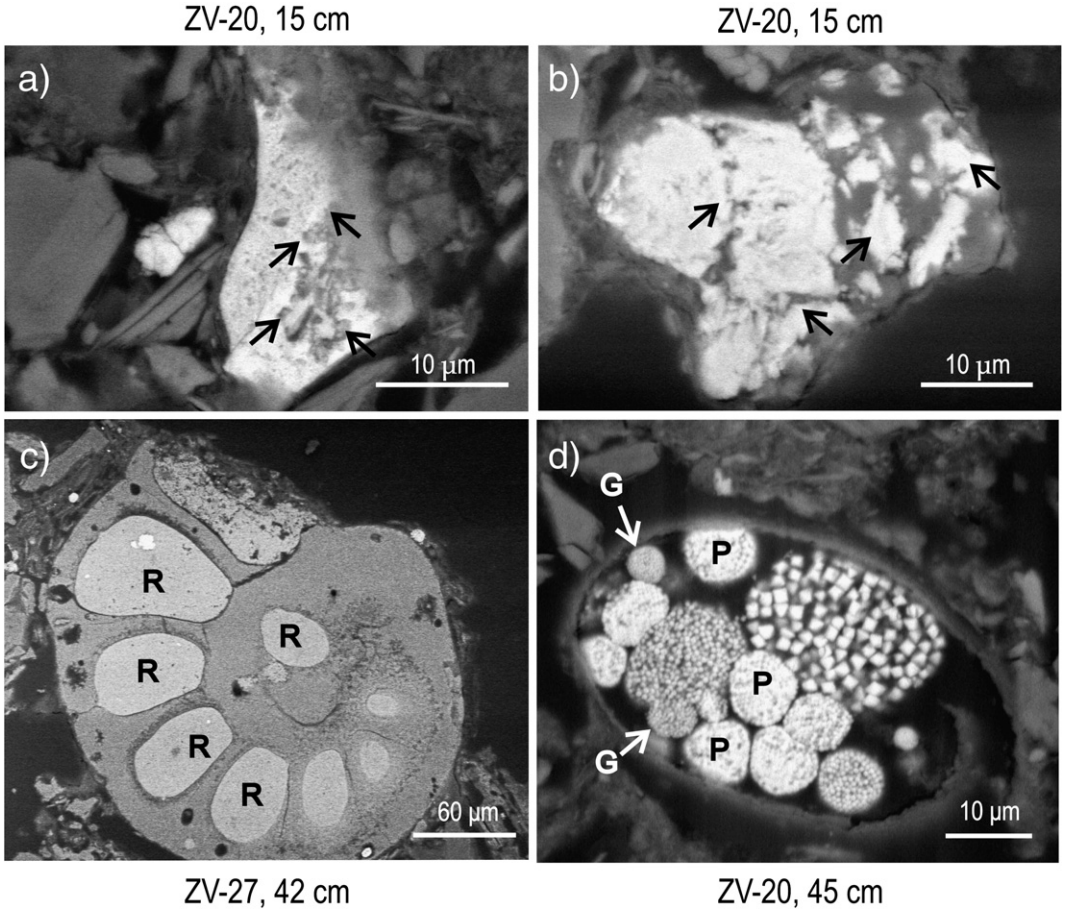

Figure 6. Representative SEM micrographs of sediments showing a) detrital iron oxides with signs of surface edging (black arrows) as a result of reductive dissolution. b) Early diagenetic reduction also causes large minerals to fragment (black arrows). c) Example showing glauconite replacements (R) in carbonate bioclasts. d) Pyrite (P) and Greigite (G) framboids coexisted in microenvironments. Labels indicate actual core and depth of sample.

southern rivers Miño and Duero (Dias et al., 2002a), this disparity can best be explained by postdepositional alteration of the detrital signal.

This alteration is caused by reductive early diagenesis, as confirmed by the SEM observation of framboidal iron sulfides, the end-product of iron reduction in marine sediments (Canfield and Berner, 1987). However, the intensity of reductive dissolution was moderate enough to allow magnetite to be present in most of the core length. This interpretation is supported by the confinement of Fe sulfides within organic-rich microenvironments and the presence of greigite, typical of mild reducing conditions (Kao et al., 2004). Greigite typically exhibits SD behavior (Roberts, 1995), which explains the small grain size decrease below peak A_1 in all the cores (Figs. 3a and b) and the more SD-like characteristics of the FORC diagrams of this region (Fig. 5c).

It can also be argued that the southern cores underwent more intense early diagenetic reductive dissolution of magnetic minerals as a result of their higher TOC contents. In this region, organic productivity is greatly enhanced by the upwelling of nutrient-rich waters forced by dominant northerly winds. Although upwelling has been intermittent throughout the Holocene (Diz et al., 2002; Martins et al., 2006), this discontinuity cannot explain these differences in TOC content because of the relatively small area affected compared to the regional influence of upwelling, extending beyond the western Iberian margin. These diagenetic differences can be explained considering lateral advection processes. Under winter conditions, the Galician Rías exhibit a well documented estuarine negative circulation pattern (deCastro et al., 2004), in which the onshore advection of water forced by southerly winds is balanced by a bottom seawards flow, transporting organic-rich fine material resuspended during southwesterly storms (Rey et al., 2005) from the Rías into the shelf. The formation of bottom nepheloid layers with high particulate organic carbon content (4–15%) after storm events is a common feature in the northern Portuguese margin (Oliveira et al., 2002) and supports the feasibility of this scenario. Local differences in the TOC export from the Rías to the shelf constrain the intensity of early redoxomorphic diagenesis at each site. In this way, the finer and more organic-rich sediments of the Ría the Vigo (Vilas et al., 2005) make cores ZV-27 and ZV-24 receive more organic matter than ZV-20 and ZV-18 in the Ría de Pontevedra, forcing the observed differences in diagenesis intensity.

Environmental significance of early diagenesis

The observed differences in the diagenetic intensity can be identified in order to better trace changes in the detrital input and in the upwelling intensity related to the climatic variability of the NW Iberian Margin during the late Holocene.

As shown previously, Unit A showed evidences of reductive early diagenesis in all the cores, which intensified downcore and towards the south. The SIRM signal decreased to half its maximum value in an average of 900 yr. This time scale is within the 50–1000 yr range proposed by Canfield and Berner (1987) for the dissolution of magnetite to half its concentration in anoxic sediments.

All the concentration-dependent magnetic properties but HIRM (more resistant to diagenesis) showed the overall negative exponential shape typical of steady-state diagenesis of Berner (1980). Therefore, we performed an exponential fit of the downcore evolution of the ferrimagnetic mineral concentration (SIRM) to represent the ideal scenario of predominant steady-state early diagenesis (Fig. 8a). This fit

https://doi.org/10.1016/j.yqres.2010.02.003 Published online by Cambridge University Press

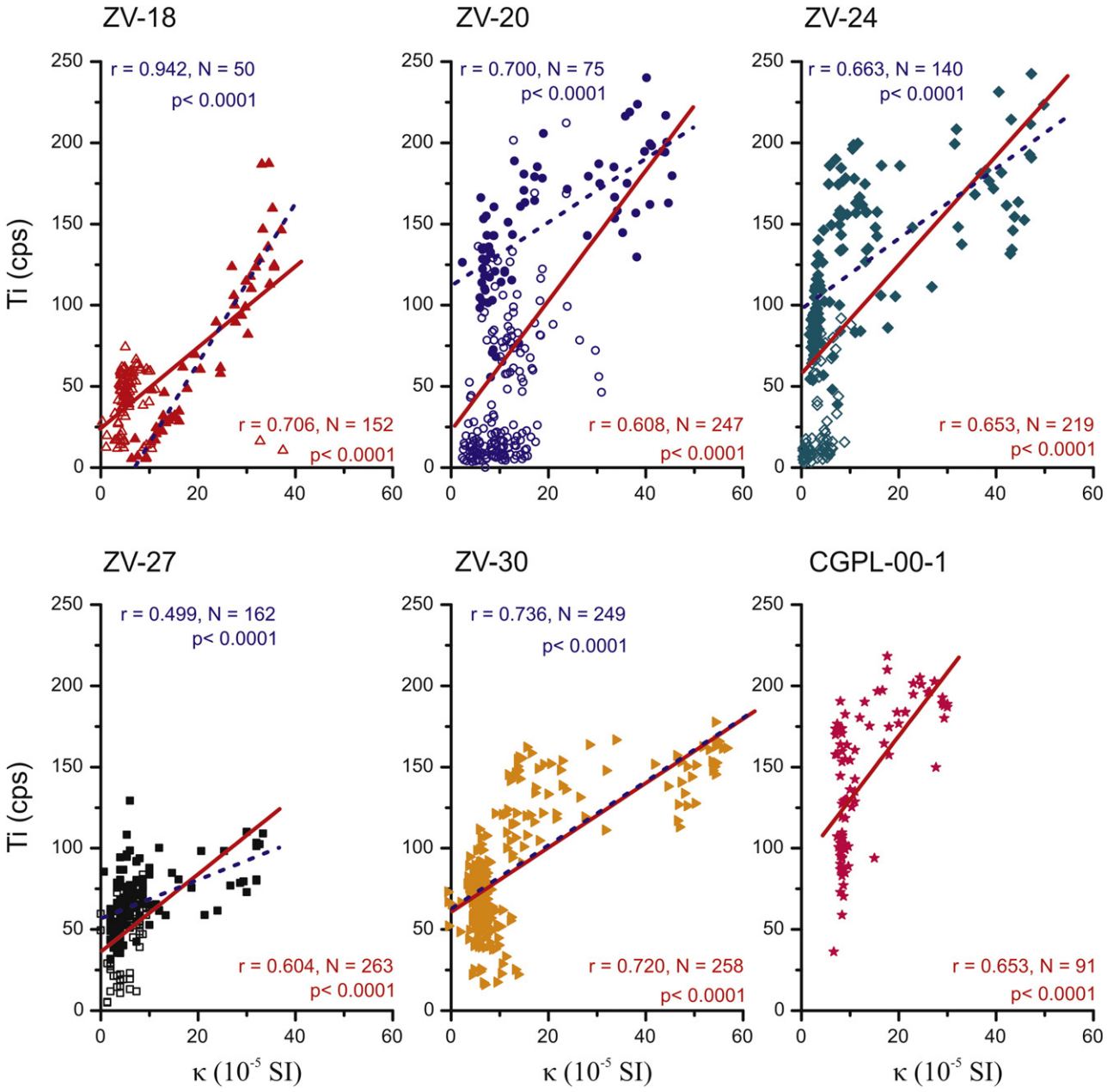

Figure 7. Plots of low-field magnetic susceptibility vs. Ti content. The red line is the linear fit for all data points in the cores. The blue line represents the fit for the data points in Unit A (solid points). Note that data scattering increases for κ below $10^{*}10^{-5}$ SI, which adds significance to the Ti-κ relationship in high-concentration magnetic zones.

was significant ($r^2 = 0.68$–0.85) and is sufficient to explain most of the observed negative exponential downcore trend. It will be demonstrated that the low-amplitude deviations from this trend are controlled by differential detrital input of magnetic minerals and their postdepositional evolution during the late Holocene, and subsequently that they can be used as proxies for environmental changes during this period.

During the RWP (~1950–1550 cal yr BP; Lamb, 1985) and the MWP (~1150–650 cal yr BP; Hughes and Diaz, 1994), values in excess of the fit indicate a local maximum in the concentration of magnetic minerals caused by enhanced continental detrital input. Similarly, values in deficit of the fit indicate magnetic concentration minima, and consequently, diminished detrital inputs and/or more intense early diagenetic dissolution. These minima are coeval with two periods of intensified upwelling in the area, the oldest spanning from 2200 cal yr BP to 1200 cal yr BP (Bartels-Jónsdóttir et al., 2006), and the most recent since 500 cal yr BP (Diz et al., 2002; Martins et al., 2007). Based on these findings, and the observed magnetomineralogical changes characteristic of reductive dissolution during these periods, we demonstrate that early diagenetic changes in the magnetic properties can be used as proxies for intensified upwelling periods. Enviromagnetic techniques complement more precise, but also more time-consuming, paleoclimatic proxies (*e.g.*, Snowball and Moros, 2003; Kleiven et al., 2008; Rey et al., 2008). Their low cost, simplicity, and speed allow the analysis of a large number of cores and therefore help to build larger databases that reinforce and validate single-core observations over a wide area, thus buttressing more accurate data with increased robustness and regional significance.

Paleoclimatic interpretation of the magnetic results

The overall decrease in detrital input with age (Fig. 8b) is actually caused by the progression of early diagenesis with depth (Fig. 8a),

https://doi.org/10.1016/j.yqres.2010.02.003 Published online by Cambridge University Press

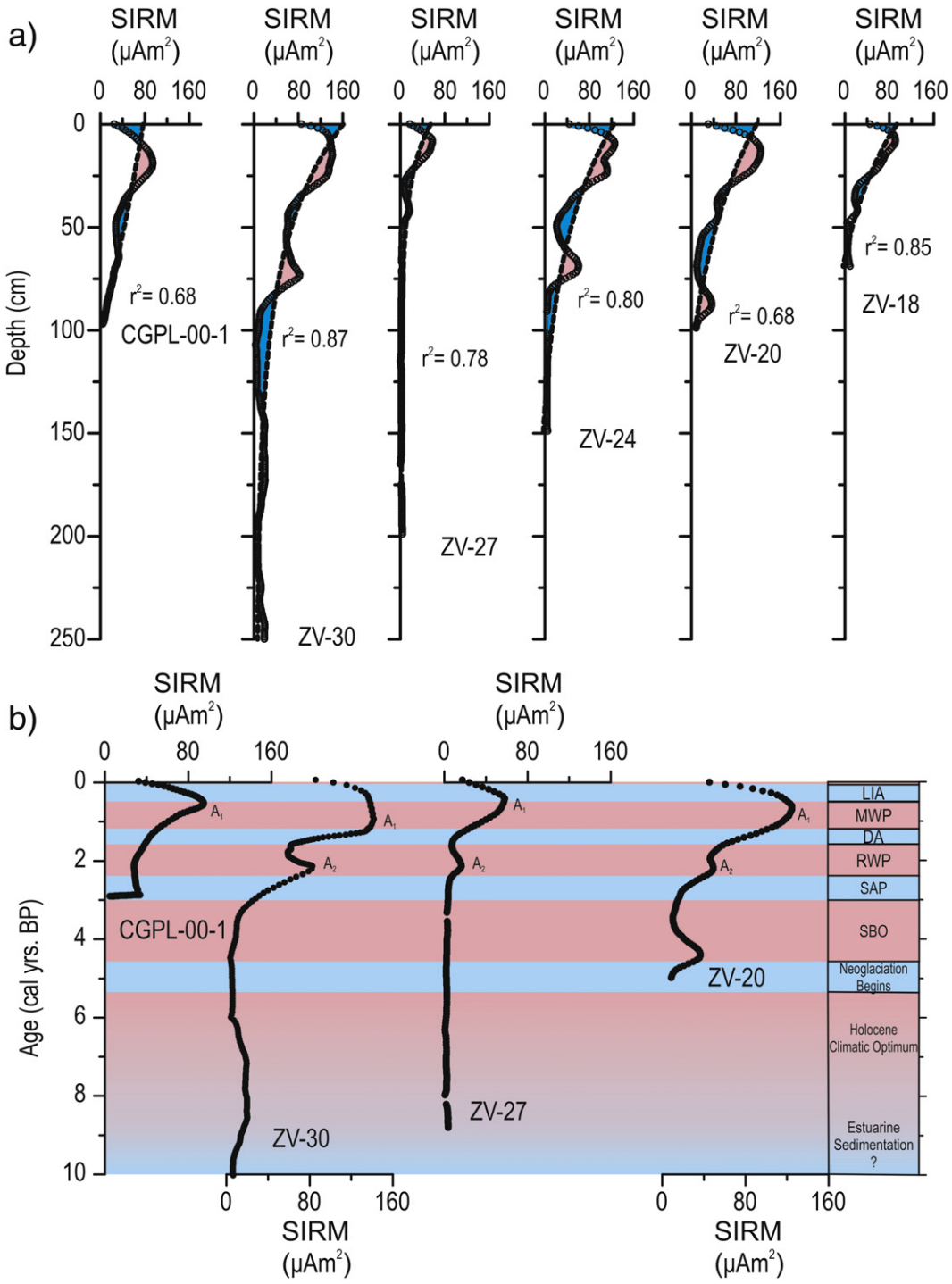

Figure 8. a) Fit of the magnetic concentration-dependent SIRM to a negative exponential representing a steady state of early diagenesis. Sediments with concentrations over the predicted value (pink) represent increased detrital input. Values below the predicted value occur in zones of lower detrital input and enhanced diagenesis (blue). b) Magnetic concentration represented in a temporal scale showed that periods of enhanced detrital input were coeval with the RWP and MWP. Therefore, higher river discharge and continental runoff in these periods caused large inputs of detrital magnetic minerals to the continental shelf. *LIA: Little Ice Age; MWP: Medieval Warm Period; DA: Dark Ages; RWP: Roman Warm Period; SAP: Sub-Atlantic Period; SBO: Sub-Boreal Optimum.*

which leads to the more effective dissolution of deeper detrital oxides, especially before the RWP (Fig. 8). It is likely that the apparent offset of the RWP in our age model towards a slightly older age (~2100 to ~2200 cal yr BP) compared to the typical 1950–1550 cal yr BP age range is a result from the enhanced dissolution of magnetic minerals during the latest part of this period, forced by the intensification of the upwelling from 2200 to 1200 cal yr BP (Bartels-Jónsdóttir et al., 2006).

However, these results clearly reveal two periods of enhanced continental input roughly coincident with the RWP and the MWP. This interpretation of the magnetic concentration peaks as the fingerprints of large detrital discharges to the continental shelf is supported by increased river runoff in the western Iberian Peninsula during the RWP (Martínez-Cortizas et al., 1999; Bernárdez et al., 2008), combined with greater erosion during the Roman colonization as a result of massive deforestation for agriculture and mining (Muñoz Sobrino et al., 2005). This enhanced continental input also explains the increase in sedimentation rates towards the south after *ca.* 2000 cal yr BP (Fig. 2), since these sites are closer to the main rivers

https://doi.org/10.1016/j.yqres.2010.02.003 Published online by Cambridge University Press

supplying sediments to the Galician Mud Patch. A lower detrital input before this period would also allow for the sediments to be more evenly distributed and would explain the similar age–depth slopes for that time interval.

After the RWP, detrital continental input to the shelf decreased until *ca.* 1200–1000 cal yr BP. This interval is coincident with a reported upwelling intensification (Bartels-Jónsdóttir et al., 2006). However, its associated productivity increase only moderately affected the magnetic properties of the southernmost cores.

From 1200–1000 cal yr BP until *ca.* 500 cal yr BP another large pulse of detrital continental material to the shelf occurred, punctuated by a small decrease roughly centered at the Little Ice Age (LIA, ~450–50 cal yr BP, *e.g.* (Bradley and Jones, 1993)). This increase in river discharge and sedimentary load during the 10th century is mentioned in historical documents (Dias et al., 2000), and also led to higher sedimentation rates in the silt deposits of the northern Portuguese continental shelf (Drago et al., 1995). These characteristics suggest increased precipitation in the northern sector of the Iberian Peninsula during the MWP, which led to increased sediment transport from the continent to the shelf. Findings of enhanced continental influence for the Ría de Vigo (Álvarez et al., 2005) and Ría de Muros (Lebreiro et al., 2006) during this period, which these authors attribute to forcings related to long NAO trends, are coherent with this interpretation. In addition, the increase in population of the northern regions of the Iberian Peninsula related to the conflicts with Muslims in the south during the MWP reinforced this effect, enhancing erosion and therefore detrital inputs to the shelf (Muñoz Sobrino et al., 2005).

Upwelling was also more intense from 500 cal yr BP (Diz et al., 2002). However, our findings suggest that its effect was not as intense on the shelf as within the Galician Rías, where magnetite can be completely dissolved within less than 50 yr (Emiroğlu et al., 2004; Mohamed, 2006). Therefore, the export of TOC to the sediment was sufficiently low as to preserve a climatically-meaningful magnetic signal for at least the last 2500 years.

Conclusions

The integrated analyses of the magnetic, geochemical and textural properties of Galician continental shelf sediments has proven to be a useful technique for detecting and tracing paleoclimatic signatures in nearshore sediments, despite the heterogeneity and the early diagenetic alteration of magnetic minerals. A conceptual model illustrating the interplay between the sedimentary characteristics of the Galician continental shelf and the processes that control them is provided in supplementary material Fig. S1.

The four sedimentary units identified since the late Pleistocene represent a succession from fluvial and subaerial coastal sediments to transgressive and high-stand marine sediments, related to the sea-level rise that occurred since the LGM.

The interplay between continental detrital input to the NW Iberian margin and the early diagenetic reductive dissolution of magnetic minerals caused two periods of high magnetic concentration during the last 2500 yr. These periods can be unambiguously traced over the studied area and their ages correspond to the RWP and MWP, and also extend into the LIA. The increased input of continental detrital minerals to the shelf was related to wetter conditions, which enhanced river discharge and sediment transport to the shelf. In addition, intense human activities in the area increased continental erosion, which favored runoff and therefore reinforced the export of sediments to the NW Iberian margin.

Magnetically depleted sediments are the result of early diagenetic dissolution of magnetic minerals. Deviations from a steady-state diagenetic trend could be used to identify periods of lower detrital input and/or enhanced upwelling. Between the RWP and the MWP, and to a lesser extent after 500 cal yr BP, enhanced upwelling and decreased detrital input to the shelf promoted the onset of reductive early diagenesis and the virtually complete dissolution of magnetic minerals. The time dependence of early diagenesis precludes the untangling of the time signal from the upwelling forcing prior to 2500 cal yr BP, where the magnetomineralogical assemblage is completely dissolved.

The southern sector of the studied region, adjacent to the Ría de Vigo, showed an increased sensitivity to reductive redox conditions. It is proposed that this is mostly due to the local accumulation of organic matter as a result of the direct export of organic matter from the Ría de Vigo by offshore bottom-currents generated during downwelling events.

These results emphasize the potential of magnetic techniques as fast, economic and high-resolution screening tools for more precise paleoenvironmental studies of the Iberian continental shelf.

Acknowledgments

Contribution to projects CTM2007-61227/MAR and REN2003-02822 funded by the Spanish MICINN. Partial contribution to projects PGIDIT06TAM31201PR and IN825B funded by Xunta de Galicia and NACSA 236962 and ANCORIM funded by the EU. The EU *Paleostudies* program funded the stay of Kais J. Mohamed in Bremen. The authors wish to thank Tilo von Dobeneck, Mark J. Dekkers and Andrew P. Roberts for their technical support and helpful discussions during the stay of K. J. Mohamed in Bremen, Utrecht and Southampton. Jerry F. McManus for his help reviewing the English and S. Brachfeld, J. Feinberg, F. Lagroix and an anonymous reviewer for their constructive comments that helped improve this paper. The authors would also like to acknowledge the assistance of R. González-Álvarez, M.S. Rúa and M. Martínez with sample preparation for ^{14}C AMS dating. K. J. Mohamed wishes to acknowledge joint funding from the Fulbright Program and the Spanish Ministry of Education and Science and the Marie Curie International Outgoing Fellowships within the 7th European Community Framework Programme. Contribution No. 394 of the University of Vigo XM2 (GEOMA) group.

Appendix A. Supplementary data

Supplementary data associated with this article can be found, in the online version, at doi:10.1016/j.yqres.2010.02.003.

References

Alonso, B., Ercilla, G., Casas, D., Estrada, F., Farrán, M., García, M., Rey, D., Rubio, B., 2008. Late Pleistocene and Holocene sedimentary facies on the SW Galicia Bank (Atlantic NW Iberian Peninsula). Marine Geology 249, 46–63.

Álvarez, M.C., Flores, J.A., Sierro, F.J., Diz, P., Francés, G., Pelejero, C., Grimalt, J., 2005. Millennial surface water dynamics in the Ría de Vigo during the last 3000 years as revealed by coccoliths and molecular biomarkers. Palaeogeography, Palaeoclimatology, Palaeoecology 218, 1–13.

Ares, A., Rey, D., Rubio, B., Mohamed, K., Bernabeu, A., Vilas, F., 2008. Reconstrucción paleoclimática de la plataforma continental gallega basada en datos geoquímicos y magnéticos. Geogaceta 44, 87–90.

Bartels-Jónsdóttir, H.B., Knudsen, K.L., Abrantes, F., Lebreiro, S., Eiríksson, J., 2006. Climate variability during the last 2000 years in the Tagus Prodelta, western Iberian Margin: benthic foraminifera and stable isotopes. Marine Micropaleontology 59, 83–103.

Bernárdez, P., González-Álvarez, R., Francés, G., Prego, R., Bárcena, M.A., Romero, O.E., 2008. Late Holocene history of the rainfall in the NW Iberian peninsula—Evidence from a marine record. Journal of Marine Systems 72, 366–382.

Berner, R.A., 1980. Early Diagenesis: A Theoretical Approach. Princeton University Press, Princeton, NJ. 241 pp.

Bloemendal, J., King, J.W., Hunt, A., Demenocal, P.B., Hayashida, A., 1993. Origin of the sedimentary magnetic record at Ocean Drilling Program Sites on the Owen Ridge, western Arabian Sea. Journal of Geophysical Research 98, 4199–4219.

Bradley, R.S., Jones, P.D., 1993. 'Little ice age' summer temperature variations: their nature and relevance to recent global warming trends. Holocene 3, 367–376.

Canfield, D.E., Berner, R.A., 1987. Dissolution and pyritization of magnetite in anoxic marine sediments. Geochimica et Cosmochimica Acta 51, 645–659.

Day, R., Fuller, M., Schmidt, V.A., 1977. Hysteresis properties of titanomagnetites: grain-size and compositional dependence. Physics of the Earth and Planetary Interiors 13, 260–267.

deCastro, M., Gomez-Gesteira, M., Alvarez, I., Prego, R., 2004. Negative estuarine circulation in the Ria of Pontevedra (NW Spain). Estuarine, Coastal and Shelf Science 60, 301–312. doi:10.1016/j.ecss.2004.01.006.
Desprat, S., Sánchez Goñi, M.F., Loutre, M., 2003. Revealing climatic variability of the last three millennia in northwestern Iberia using pollen influx data. Earth and Planetary Science Letters 213, 63–78.
Dias, J.M.A., Boski, T., Rodrigues, A., Magalhães, F., 2000. Coast line evolution in Portugal since the Last Glacial Maximum until present — a synthesis. Marine Geology 170, 177–186.
Dias, J.M.A., Gonzalez, R., Garcia, C., Diaz-del-Rio, V., 2002a. Sediment distribution patterns on the Galicia-Minho continental shelf. Progress in Oceanography 52, 215–231.
Dias, J.M.A., Jouanneau, J.M., Gonzalez, R., Araújo, M.F., Drago, T., Garcia, C., Oliveira, A., Rodrigues, A., Vitorino, J., Weber, O., 2002b. Present day sedimentary processes on the northern Iberian shelf. Progress in Oceanography 52, 249–259. doi:10.1016/S0079-6611(02)00009-5.
Diz, P., Frances, G., Pelejero, C., Grimalt, J.O., Vilas, F., 2002. The last 3000 years in the Ria de Vigo (NW Iberian Margin): climatic and hydrographic signals. The Holocene 12, 459–468. doi:10.1191/0959683602hl550rp.
Drago, T., Jouanneau, J.M., Dias, J.M.A., Prud'Homme, R., 1995. Os factores condicionantes da existencia e alimentaçao do complexo silto-argiloso situado a Oeste do Douro. Memórias do Museu Laboratório Mineralógico e Geológico da Facultade de Ciencias do Porto 41, 917–921.
Drago, T., Oliveira, A., Magalhães, F., Cascalho, J., Jouanneau, J.-, Vitorino, J., 1998. Some evidences of northward fine sediment transport in the northern Portuguese continental shelf. Oceanologica Acta 21, 223–231.
Dunlop, D.J., 2002a. Theory and application of the Day plot (Mrs/Ms versus Hcr/Hc) 1. Theoretical curves and tests using titanomagnetite data. Journal of Geophysical Research 107, 2056. doi:10.1029/2001JB000486.
Dunlop, D.J., 2002b. Theory and application of the Day plot (Mrs/Ms versus Hcr/Hc) 2. Application to data for rocks, sediments, and soils. Journal of Geophysical Research B: Solid Earth 107, 5-1.
Durán, R., 2005. Estratigrafía sísmica desde el último máximo glacial en la Ría de Pontevedra (NO España). Universidade de Vigo, Vigo. 300 pp.
Emiroğlu, S., Rey, D., Petersen, N., 2004. Magnetic properties of sediment in the Ría de Arousa (Spain): dissolution of iron oxides and formation of iron sulphides. Physics and Chemistry of the Earth, Parts A/B/C 29, 947–959.
Evans, M.E., Heller, F., 2003. Environmental Magnetism: Principles and Applications of Enviromagnetics. Academic Press (Elsevier), New York. 299 pp.
Fernández-Bastero, S., Velo, A., García, T., Gago-Duport, L., Santos, A., García-Gil, S., Vilas, F., 2000. Las glauconitas de la plataforma continental gallega: indicadores geoquímicos del grado de evolución. Journal of Iberian Geology 26, 233–247.
Fraga, F., 1981. Upwelling off the Galician coast, Northwest Spain. In: Richards, F.A. (Ed.), Coastal Upwelling Series, 1. American Geophysical Union, Washington, DC, pp. 176–182.
García-García, A., García-Gil, S., Vilas, F., 2005. Quaternary evolution of the Ría de Vigo, Spain. Marine Geology 220, 153–179.
González-Álvarez, R., Francés, G., 2005. Paleoenvironmental conditions of the Galician continental shelf during the Holocene. In: Freitas, M.C., Drago, T. (Eds.), Coastal HOPE 2005 Proceedings, pp. 74–75.
González-Álvarez, R., Bernárdez, P., Pena, L.D., Francés, G., Prego, R., Diz, P., Vilas, F., 2005. Paleoclimatic evolution of the Galician continental shelf (NW of Spain) during the last 3000 years: from a storm regime to present conditions. Journal of Marine Systems 54, 245–260.
Hughen, K.A., Baillie, M.G.L., Bard, E., Bayliss, A., Beck, J.W., Bertrand, C.J.H., Blackwell, P.G., Buck, C.E., Burr, G.S., Cutler, K.B., Damon, P.E., Edwards, R.L., Fairbanks, R.G., Friedrich, M., Guilderson, T.P., Kromer, B., McCormac, F.G., Manning, S.W., Bronk Ramsey, C., Reimer, P.J., Reimer, R.W., Remmele, S., Southon, J.R., Stuiver, M., Talamo, S., Taylor, F.W., van der Plicht, J., Weyhenmeyer, C.E., 2004. Marine04 marine radiocarbon age calibration, 0–26 cal kyr BP. Radiocarbon 46, 1059–1086.
Hughes, M.K., Diaz, H.F., 1994. Was there a 'medieval warm period', and if so, where and when? Climatic Change 26, 109–142. doi:10.1007/BF01092410.
Hurrell, J.W., Kushnir, Y., Visbeck, M., 2001. The North Atlantic Oscillation. Science 291, 603–605.
Justino, F., Peltier, W.R., 2005. The glacial North Atlantic Oscillation. Geophysical Research Letters 32, 1–4.
Kao, S.-J., Horng, C.-S., Roberts, A.P., Liu, K.-K., 2004. Carbon–sulfur–iron relationships in sedimentary rocks from southwestern Taiwan: influence of geochemical environment on greigite and pyrrhotite formation. Chemical Geology 203, 153–168.
Kleiven, H.F., Kissel, C., Laj, C., Ninnemann, U.S., Richter, T.O., Cortijo, E., 2008. Reduced North Atlantic deep water coeval with the glacial Lake Agassiz freshwater outburst. Science 319, 60–64. doi:10.1126/science.1148924.
Kruiver, P.P., Dekkers, M.J., Heslop, D., 2001. Quantification of magnetic coercivity components by the analysis of acquisition curves of isothermal remanent magnetisation. Earth and Planetary Science Letters 189, 269–276.
Lamb, H.H., 1985. Climate History and the Future. Princeton University Press, Princeton, NJ. 835 pp.
Larrasoaña, J.C., Roberts, A.P., Stoner, J.S., Richter, C., Wehausen, R., 2003. A new proxy for bottom-water ventilation in the eastern Mediterranean based on diagenetically controlled magnetic properties of sapropel-bearing sediments. Palaeogeography, Palaeoclimatology, Palaeoecology 190, 221–242.
Lebreiro, S.M., Francés, G., Abrantes, F.F.G., Diz, P., Bartels-Jónsdóttir, H.B., Stroynowski, Z.N., Gil, I.M., Pena, L.D., Rodrigues, T., Jones, P.D., Nombela, M.A., Alejo, I., Briffa, K.R., Harris, I., Grimalt, J.O., 2006. Climate change and coastal hydrographic response along the Atlantic Iberian margin (Tagus Prodelta and Muros Ría) during the last two millennia. Holocene 16, 1003–1015.
Lesueur, P., Tastet, J.P., Weber, O., 2002. Origin and morphosedimentary evolution of fine-grained modern continental shelf deposits: the Gironde mud fields (Bay of Biscay, France). Sedimentology 49, 1299–1320.
Liu, J., Zhu, R., Roberts, A.P., Li, S., Chang, J., 2004. High-resolution analysis of early diagenetic effects on magnetic minerals in post-middle-Holocene continental shelf sediments from the Korea Strait. Journal of Geophysical Research B: Solid Earth 109, B03103. doi:10.1029/2003JB002813.
Martínez-Cortizas, A., Valcarcel-Díaz, M., Pérez-Alberti, A., Castillo-Rodríguez, F., Blanco-Chao, R., 1999. O cambio climático e os paleoclimas cuaternarios. In: Martínez-Cortizas, A., Pérez-Alberti, A. (Eds.), Atlas climático de Galicia. Consellería de Medioambiente. Xunta de Galicia, Santiago de Compostela, pp. 167–185.
Martins, V., Jouanneau, J., Weber, O., Rocha, F., 2006. Tracing the late Holocene evolution of the NW Iberian upwelling system. Marine Micropaleontology 59, 35–55.
Martins, V., Dubert, J., Jouanneau, J., Weber, O., da Silva, E.F., Patinha, C., Alveirinho Dias, J.M., Rocha, F., 2007. A multiproxy approach of the Holocene evolution of shelf–slope circulation on the NW Iberian Continental Shelf. Marine Geology 239, 1–18.
Mohamed, K.J., 2006. Influencia climática, diagenética y antropogénica sobre la señal magnética y geoquímica de los sedimentos marinos cuaternarios del noroeste de la Península Ibérica. Ph.D. Thesis, Faculty of Marine Sciences, University of Vigo, Vigo, Spain. 298 pp.
Muñoz Sobrino, C., Ramil-Rego, P., Gómez-Orellana, L., Varela, R.A.D., 2005. Palynological data on major Holocene climatic events in NW Iberia. Boreas 34, 381–400.
Nagata, T., Carleton, B.J., 1987. Magnetic remanence coercivity of rocks. Journal of Geomagnetism and Geoelectricity 39, 447–461.
Oliveira, A., Rocha, F., Rodrigues, A., Jouanneau, J., Dias, A., Weber, O., Gomes, C., 2002. Clay minerals from the sedimentary cover from the northwest Iberian shelf. Progress in Oceanography 52, 233–247. doi:10.1016/S0079-6611(02)00008-3.
Passier, H.F., De Lange, G.J., Dekkers, M.J., 2001. Magnetic properties and geochemistry of the active oxidation front and the youngest sapropel in the eastern Mediterranean sea. Geophysical Journal International 145, 604–614.
Postma, H., 1967. Sediment transport and sedimentation in the estuarine environment. In: Lauff, G.H. (Ed.), Estuaries. American Association for the Advancement of Science, Washington DC, pp. 651–658.
Rey, J., 1993. Relación morfosedimentaria entre la plataforma continental de Galicia y las Rías Baixas y su evolución durante el Cuaternario. Instituto Español de Oceanografía, Madrid, España. 233 pp.
Rey, D., Mohamed, K.J., Bernabeu, A., Rubio, B., Vilas, F., 2005. Early diagenesis of magnetic minerals in marine transitional environments: geochemical signatures of hydrodynamic forcing. Marine Geology 215, 215–236.
Rey, D., Rubio, B., Mohamed, K., Vilas, F., Alonso, B., Ercilla, G., Rivas, T., 2008. Detrital and early diagenetic processes in Late Pleistocene and Holocene sediments from the SW Galicia Bank inferred from high-resolution enviromagnetic and geochemical records. Marine Geology 249, 64–92.
Roberts, A.P., 1995. Magnetic properties of sedimentary greigite (Fe3S4). Earth and Planetary Science Letters 134, 227–236. doi:10.1016/0012-821X(95)00131-U.
Roberts, A.P., Pillans, B.J., 1993. Rock magnetism of Lower Middle Pleistocene marine sediments, Wanganui Basin, New Zealand. Geophysical Research Letters 20, 839–842.
Roberts, A.P., Weaver, R., 2005. Multiple mechanisms of remagnetization involving sedimentary greigite (Fe3S4). Earth and Planetary Science Letters 231, 263–277.
Sagnotti, L., Roberts, A.P., Weaver, R., Verosub, K.L., Florindo, F., Pike, C.R., Clayton, T., Wilson, G.S., 2005. Apparent magnetic polarity reversals due to remagnetization resulting from late diagenetic growth of greigite from siderite. Geophysical Journal International 160, 89–100.
Snowball, I., Moros, M., 2003. Saw-tooth pattern of North Atlantic current speed during Dansgaard-Oeschger cycles revealed by the magnetic grain size of Reykjanes Ridge sediments at 59°N. Paleoceanography 18, 4-1.
Stuiver, M., Reimer, P.J., 1993. Extended 14C data base and revised CALIB 3.0 14C age calibration program. Radiocarbon 35, 215–230.
Thompson, R., Oldfield, F., 1986. Environmental Magnetism. Allen and Unwin, London, UK. 227 pp.
Vilas, F., Bernabeu, A., Rubio, B., Rey, D., 2010. Estuarios, rías y llanuras intermareales. In: Arche, A. (Ed.), Sedimentología: del proceso físico a la cuenca sedimentaria. Publicaciones del CSIC, Madrid, pp. 621–675.
Vilas, F., Bernabeu, A.M., Méndez, G., 2005. Sediment distribution pattern in the Rias Baixas (NW Spain): main facies and hydrodynamic dependence. Journal of Marine Systems 54, 261–276.
Winklhofer, M., Zimanyi, G.T., 2006. Extracting the intrinsic switching field distribution in perpendicular media: a comparative analysis. Journal of Applied Physics 99 (8) 08E710-1-3.